Hindawi
International Transactions on Electrical Energy Systems
Volume 2024, Article ID 5526545, 12 pages
https://doi.org/10.1155/2024/5526545

Research Article

A Robust Regenerative-Braking Control of Induction Motors for EVs Applications

Omar E. M. Youssef,[1,2] Mohamed G. Hussien ,[3,4] and Abd El-Wahab Hassan[2,4]

[1]*Electrical Engineering Department, Faculty of Engineering at Shoubra, Benha University, Cairo, Egypt*
[2]*Department of Electrical Power and Machines Engineering, Higher Institute of Engineering (HIE), El-Shorouk Academy, El-Shorouk City, Egypt*
[3]*School of Mechanical Engineering and Automation, Harbin Institute of Technology (Shenzhen), Shenzhen, China*
[4]*Department of Electrical Power and Machines Engineering, Faculty of Engineering, Tanta University, Tanta, Egypt*

Correspondence should be addressed to Mohamed G. Hussien; mohamed.hussien3@f-eng.tanta.edu.eg

Received 21 August 2023; Revised 7 December 2023; Accepted 1 February 2024; Published 12 February 2024

Academic Editor: Flah Aymen

EVs suffer from short driving range because of limited capacity of the battery. An advantage of EVs over internal-combustion vehicles is the ability of regenerative braking (RB). By this advantage, EVs can develop energy by RB which can be stored in the battery for later use to increase the driving range of EVs. There are different motors that can be used in EVs, and the control during RB mode is dedicated for certain motor types. However, the previous studies for EV-based IM drives consider the motor-speed control without considering its RB. This paper proposes a robust control of induction motor (IM) during RB mode of EVs. The proposed control system is simple and depends only on mathematical calculations. The obtained results confirm the effectiveness and accuracy of the suggested control strategy with a good dynamic behavior under different operating conditions. Also, the results assure the robustness of control capabilities under parameters uncertainties during the RB mode of EV-based IM drives.

1. Introduction

Electric vehicles (EVs) play a pivotal role in mitigating carbon emissions and fostering a low-carbon future. By relying on electricity as a power source, EVs significantly reduce reliance on traditional fossil fuels, thereby lowering the carbon footprint associated with transportation [1]. The integration of renewable energy sources for electricity generation further enhances the environmental benefits of EVs. As the grid becomes increasingly powered by renewable energy, the overall lifecycle emissions of electric vehicles continue to decrease [2, 3]. This symbiotic relationship between electric vehicles and a low-carbon future underscores the transformative potential of clean transportation in the global effort to combat climate change. The adoption and advancement of electric vehicles represent a crucial step towards achieving sustainable, low-carbon mobility on a large scale.

The integration of autonomous driving technology in electric vehicles represents a significant leap forward in enhancing overall efficiency and sustainability in the automotive industry. By combining the advancements in electric propulsion with autonomous capabilities, these vehicles offer a seamless and intelligent transportation solution [4]. Autonomous electric vehicles (AEVs) have the potential to optimize energy consumption, improve traffic flow, and reduce environmental impact [5, 6]. The efficiency gains stem from the ability of autonomous systems to optimize route planning, adapt driving behavior to real-time traffic conditions, and maximize energy recovery through regenerative braking. Moreover, autonomous driving can enhance safety by mitigating human errors, leading to a reduction in accidents. This synergy between autonomy and electric propulsion not only redefines the driving experience but also contributes to a more sustainable and efficient future for urban mobility.

Efforts to replace internal-combustion-engine vehicles with electric vehicles (EVs) are motivated by environmental concerns which encourage increasing of renewable energy usage and decreasing of fossil fuel consumption [7, 8]. EVs can depend on renewable energy sources, and propulsion of EVs is through powertrains of higher efficiency [9, 10]. A weakness of EVs is the relatively short driving range because of limited capacity of the battery [11, 12]. This weakness can be alleviated by increasing the efficiency of EVs using regenerative braking (RB), which is an advantage of EV over internal-combustion vehicle. Using RB, the kinetic energy of the vehicle can be converted to electrical energy, instead of wasted as heat by friction braking, and this energy is stored in the battery for later use [9]. During braking of EVs, the braking force is applied on both the front axle and rear axle of the vehicle [13, 14]. The division of the braking force between the two axles may be according to the ideal braking-force-distribution curve for best stability, or other braking-force distribution methods for improved recovered braking energy [15, 16].

In general, braking systems include both the friction braking and RB. This is because RB is insufficient at high braking requirements and at low ability of the battery to store the generated energy, where the regeneration is inappropriate once the battery is fully charged [17, 18]. For emergency braking, only the friction braking is used to obtain a safe braking, and there is no recovered energy [17, 18]. Also, the regeneration is inappropriate at low-speed values because the power is supplied by the battery instead of stored in it. The low-speed cutoff point (LSCP), below which RB is disabled, may be taken as a fixed value, or a varied value according to the operating conditions.

For a front-wheel drive EV, the rear braking force is only exerted by friction braking, and the front-braking force is shared between the friction barking and RB, where the demanded RB force is bounded according to the maximum value of the motor-braking torque. The general configuration of regenerative-braking strategies of the front-wheel drive EV can be as shown in Figure 1 [19, 20]. By pressing the braking pedal, the value of so-called barking intensity (z) is determined, and this value is used to determine the braking-force distribution between the front axle and rear axle of the vehicle. The rear braking force (f_r) is a friction force, while the front-braking force (f_f) is divided into friction-front-braking force ($f_{f,f}$) and regenerative-braking force ($f_{f,\mathrm{reg}}$) by a front-braking-force distribution controller. The operation of this controller is depending on braking situation (emergency braking or not), and the values of the speed, state of charge and maximum motor-braking torque ($T_{\max}$), which is corresponding to the force value $F_{\max}$. The operation of this controller can be as shown in Figure 2. The force $f_{f,\mathrm{reg}}$ is used to estimate regenerative-braking torque which is the reference torque (T_{ref}) used by the motor control. The motor control is a regenerative-braking control that is dedicated for a certain motor. In [21], the motor-regenerative-braking control is optimized for switched reluctance motor (SRM). In [7, 20], the control is enhanced for brushless dc (BLDC) motor, and in [22], it is enhanced for permanent-magnet synchronous motor (PMSM). However, it seems that there are no thoughtful attempts to obtain dedicated control for induction motor during regenerative braking, although there is dedicated speed control such as in [13, 23].

This paper proposes a control scheme of three-phase induction motor (IM) for the regenerative-braking operation of EVs. The adopted control scheme is simple, which leads to easy implementation. Also, there is no need of core machine parameters in the control procedure, and this will increase the robustness of the control performance during the regenerative-braking mode. Moreover, the control of induction motor during the regenerative-braking mode has not been considered in the previous studies for EV-based IM drives.

2. Mechanical System

The mechanical equation can be given by [24, 25]

$$T_d = T_{Lq} + B_m\omega_m + J_{eq}\frac{d\omega_m}{\mathrm{d}t}, \tag{1}$$

where ω_m is the mechanical angular speed, T_d is the driving torque, T_{Leq} is the equivalent load torque, J_{eq} is the equivalent inertia of the vehicle, and B_m is the friction coefficient.

In RB operation, T_d is a negative value equal to the equivalent total braking torque (T_{brake}), corresponding to total braking force ($f_f + f_r$), where

$$T_{\mathrm{brake}} = T_f + T_r, \tag{2}$$

$$T_f = T_{f,f} + T_{f,\mathrm{reg}}, \tag{3}$$

where T_f is the front-braking torque (corresponding to f_f), T_r is the rear braking torque (corresponding to f_r), $T_{f,f}$ is the friction-front-braking torque (corresponding to $T_{f,f}$), and $T_{f,\mathrm{reg}}$ is the regenerative-front-braking torque (analogous to $f_{f,\mathrm{reg}}$).

The value of $T_{f,\mathrm{reg}}$ is taken as a reference value for the motor control (T_{ref}). Thus,

$$T_{\mathrm{ref}} = T_{f,\mathrm{reg}}, \tag{4}$$

$$T_{\mathrm{ref}} = T_{\mathrm{brake}} - T_r - T_{f,f}. \tag{5}$$

3. Proposed Regenerative-Braking Control System

Many control loops were used for enhancing the electric motor drive and the vehicle efficiency. The major of these researchers were exposed a standard control loops as it is in [26, 27]. Other intelligent control topologies were exposed in [28, 29], where deep learning is used for enhancing the efficiency of the electrical motor generator.

Predictive control and sliding mode control forms were also exposed in many applications for enhancing the overall system as it is in [30, 31]

From the other side, Kalman filter was used in many applications in order to enhance the system control loop and this reference can give an example [32].

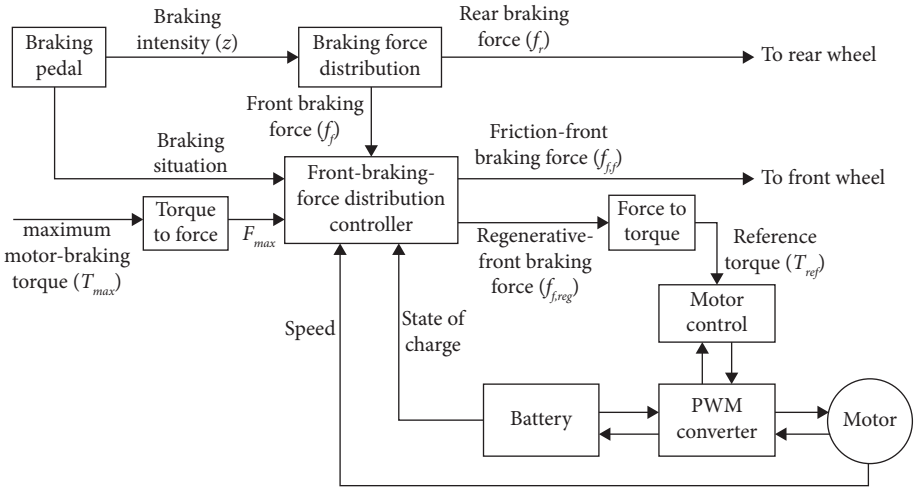

Figure 1: General configuration of regenerative-braking strategies of the front-wheel drive of EV.

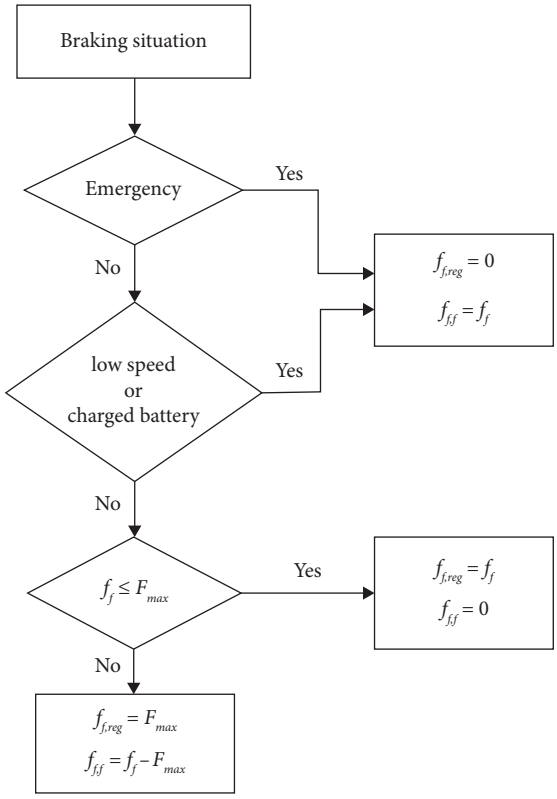

Figure 2: Operation of a front-braking-force distribution controller.

In the proposed control system, the regenerative-braking operation of the induction motor is obtained according to the reference values T_{ref} and $\lambda_{s,\text{ref}}$. The outputs of the control system are the reference stator voltages ($u_{\text{qs}(\lambda),\text{ref}}$ and $u_{\text{ds}(\lambda),\text{ref}}$), where the subscript ($\lambda$) is used to indicate the stator-flux frame. The low-speed cutoff point (LSCP) considered here is taken as a fixed value. Once this speed is reached, the reference values T_{ref} and $\lambda_{s,\text{ref}}$ are taken equal to zero. The complete motor control system is shown in Figure 3.

3.1. Calculation of Reference D-Axis Voltage ($u_{ds(\lambda),ref}$). The d-axis component of the stator voltage ($u_{\text{ds}(\lambda)}$) can be given by

$$u_{\text{ds}(\lambda)} = R_s\, i_{\text{ds}(\lambda)} + \frac{d\lambda_s}{dt}, \tag{6}$$

where R_s is the stator resistance, $i_{\text{ds}(\lambda)}$ is the d-axis component of stator current in the stator-flux frame, and λ_s is the stator flux.

The proposed reference voltage $u_{\text{ds}(\lambda),\text{ref}}$, appropriate to obtain the reference stator flux $\lambda_{s,\text{ref}}$, is obtained by

$$u_{\text{ds}(\lambda),\text{ref}} = u_{Rs} + \frac{\lambda_{s,\text{ref}} - \lambda_s}{\Delta t}, \tag{7}$$

where

$$u_{\text{Rs}} = \text{sign}\left(\lambda_{s,\text{ref}} - \lambda_s\right)\frac{\lambda_{s,\text{ref}}}{\lambda_s}\left|u_{\text{RsO}}\right|, \tag{8}$$

$$u_{\text{RsO}} = u_{\text{ds}(\lambda),\text{refO}} - \frac{\lambda_{s,\text{refO}} - \lambda_{sO}}{\Delta t}, \tag{9}$$

where Δt is the time step of estimation, u_{Rs} is the voltage drop across the resistance R_s, u_{RsO} is the voltage drop across the resistance R_s at time (t-Δt), $u_{\text{ds}(\lambda),\text{refO}}$ is the reference d-axis voltage at time (t-Δt), $\lambda_{s,\text{refO}}$ is the reference stator flux at time (t-Δt), and λ_{sO} is the stator flux at time (t-Δt).

The stator flux (λ_s) and its angle (θ_λ), in the stationary reference frame, can be obtained as follows:

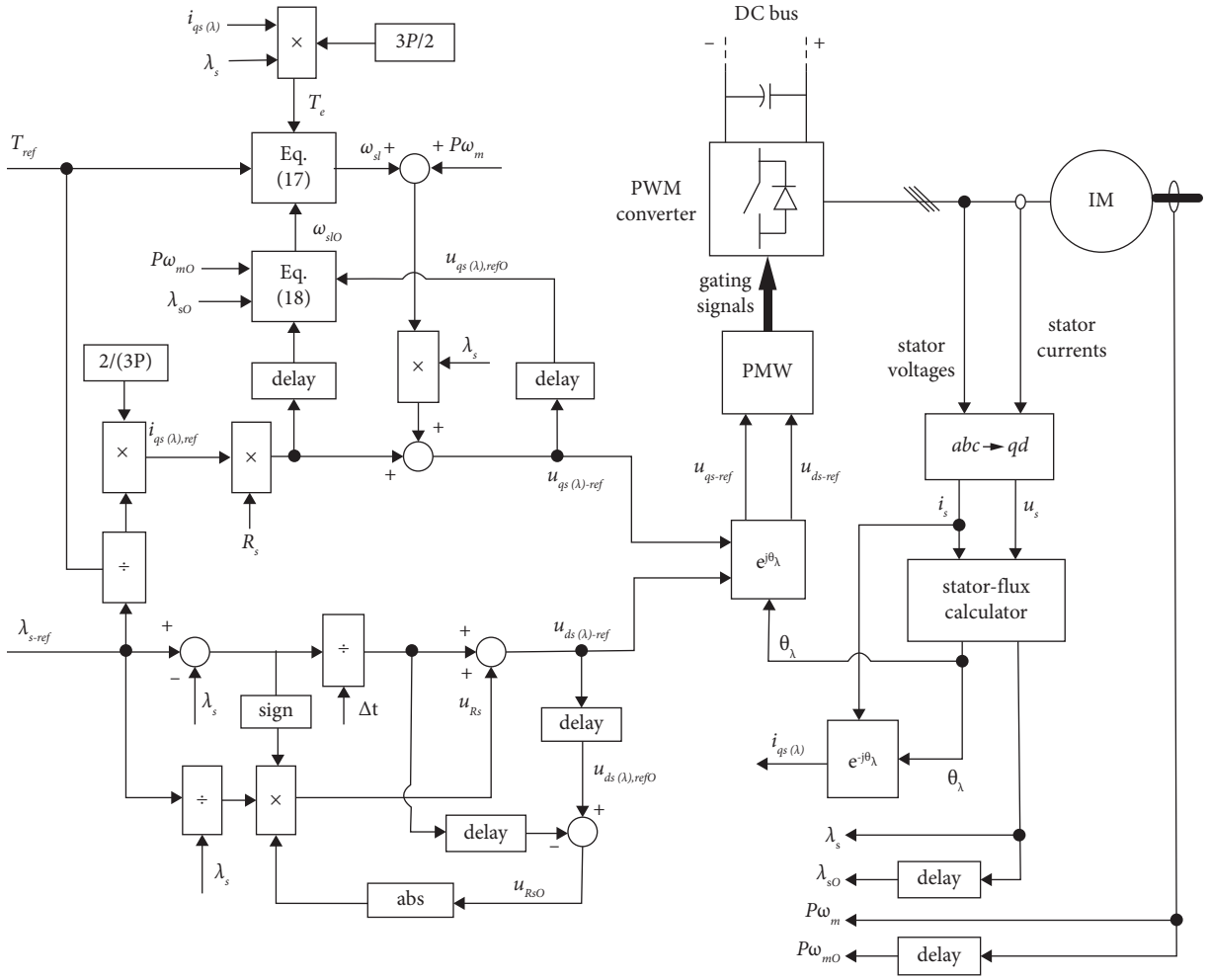

Figure 3: Proposed motor control system during RB mode.

$$\lambda_{qs} = \int \left(u_{qs} - R_s\, i_{qs}\right) \mathrm{d}t, \tag{10}$$

$$\lambda_{ds} = \int \left(u_{ds} - R_s\, i_{ds}\right) \mathrm{d}t, \tag{11}$$

$$\lambda_s = \sqrt{{\lambda_{qs}}^2 + {\lambda_{ds}}^2}, \tag{12}$$

$$\theta_\lambda = \tan^{-1}\left(\frac{\lambda_{qs}}{\lambda_{ds}}\right), \tag{13}$$

where λ, u, and i mean stator flux, voltage, and current, respectively, and the subscripts mean q-axis and d-axis components.

It should be noted that the integration is applied in the implementation process using the discrete calculations.

3.2. Calculation of Reference Q-Axis Voltage ($u_{qs(\lambda),ref}$). The q-axis component of the stator voltage ($u_{\mathrm{qs}(\lambda)}$) can be given by

$$u_{qs(\lambda)} = R_s\, i_{\mathrm{qs}(\lambda)} + \omega_e \lambda_s, \tag{14}$$

where $i_{\mathrm{qs}(\lambda)}$ is the q-axis component of stator current and ω_e is the angular speed of the stator-flux reference frame.

The proposed reference voltage $u_{\mathrm{qs}(\lambda),\mathrm{ref}}$, appropriate to obtain the reference torque T_{ref}, is obtained by

$$u_{\mathrm{qs}(\lambda),\mathrm{ref}} = R_s\, i_{\mathrm{qs}(\lambda),\mathrm{ref}} + \left(P\,\omega_m + \omega_{\mathrm{sl}}\right)\lambda_s, \tag{15}$$

where

$$i_{qs(\lambda),\mathrm{ref}} = \frac{2}{3P\,\lambda_{s,\mathrm{ref}}}\, T_{\mathrm{ref}}, \tag{16}$$

$$\begin{cases} \omega_{sl} = -\dfrac{T_{\mathrm{ref}}}{T_e}\left|\omega_{slO}\right|, & T_e < 0 \ (\text{as } T_{\mathrm{ref}}), \\ \omega_{sl} = -\left(\dfrac{\left|T_{\mathrm{ref}}\right| + T_e}{T_e}\right)\left|\omega_{slO}\right|, & T_e > 0, \end{cases} \tag{17}$$

$$\omega_{\mathrm{slO}} = \frac{u_{\mathrm{qs}(\lambda),\mathrm{ref}O} - R_s\, i_{\mathrm{qs}(\lambda),\mathrm{ref}O}}{\lambda_{sO}} - P\omega_{mO}, \tag{18}$$

$$T_e = \frac{3}{2} P\, \lambda_s\, i_{\mathrm{qs}(\lambda)}, \tag{19}$$

Table 1: Data of three-phase induction motor: star-connected, 100 hp, 460 V, 107 A, 1764 rpm, and 60 Hz.

Stator resistance (R_s)	0.06 Ω
Rotor resistance (R_r)	0.05 Ω
Stator leakage inductance (L_{ls})	0.435 mH
Rotor leakage inductance (L_{lr})	0.435 mH
Magnetizing inductance (L_m)	22.6 mH
Equivalent inertia of the vehicle at full load	44 kg m^2
Total friction coefficient	0.011 Nms/rad

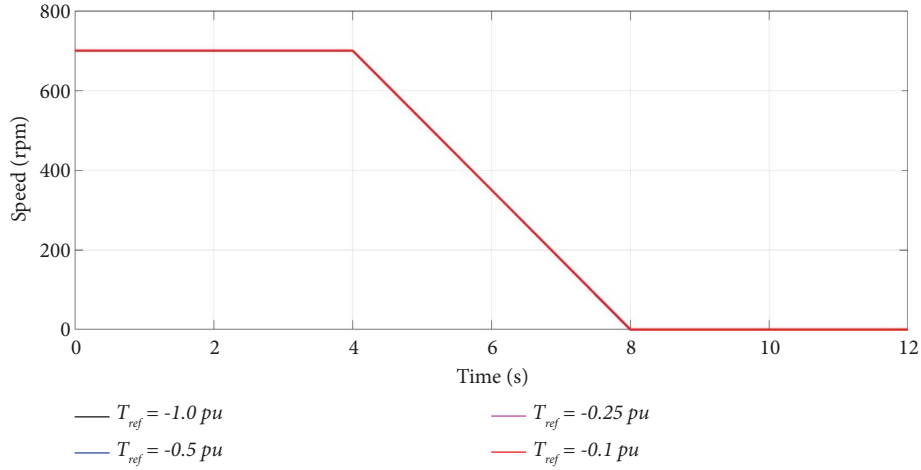

Figure 4: Motor speed.

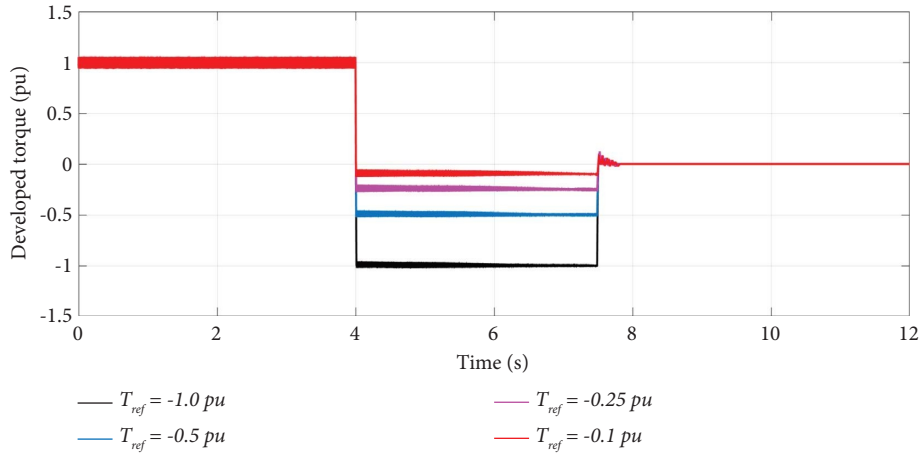

Figure 5: Developed torque.

where P is the number of pole pairs, $i_{qs(\lambda)}$ is the q-axis component of stator current, ω_{sl} is the angular slip speed, ω_{slO} is the angular slip speed at time (t-Δt), $u_{qs(\lambda),refO}$ is the reference q-axis voltage at time (t-Δt), and ω_{mO} is the angular speed at time (t-Δt).

In the second expression of equation (17), the numerator is increased by the value T_e because when the sign of T_e is changed from negative to positive, the difference between T_{ref} (negative value) and T_e is increased by the value T_e.

4. Results and Discussion

In order to ensure the effectiveness of the proposed control system, 100 hp induction motor is used with the complete parameters given in Table 1. Results are obtained when the total braking torque (T_{brake}) is equal to −1.0 pu, the equivalent load torque (T_{Leq}) is equal to 1.0 pu, and the low-speed cutoff point (LSCP) is taken equal to 90 rpm. There are different values of the reference torque (T_{ref}), which is a part

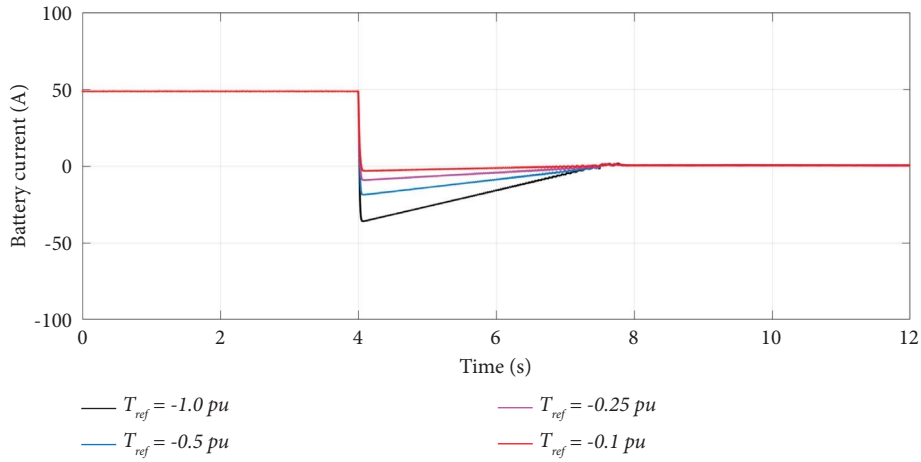

Figure 6: Battery current.

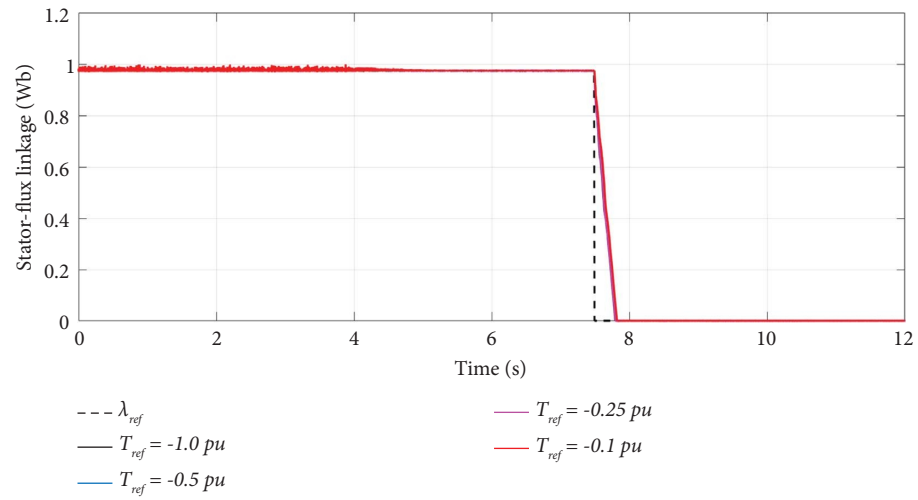

Figure 7: Stator-flux linkage.

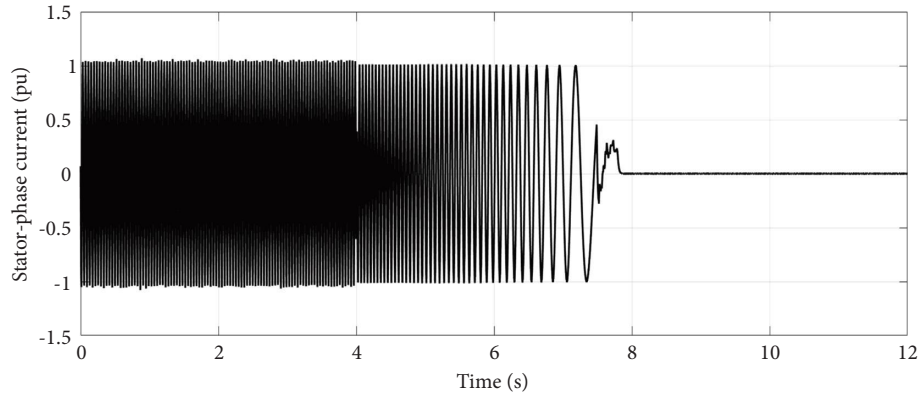

Figure 8: Motor current when $T_{\text{ref}} = -1.0$ pu.

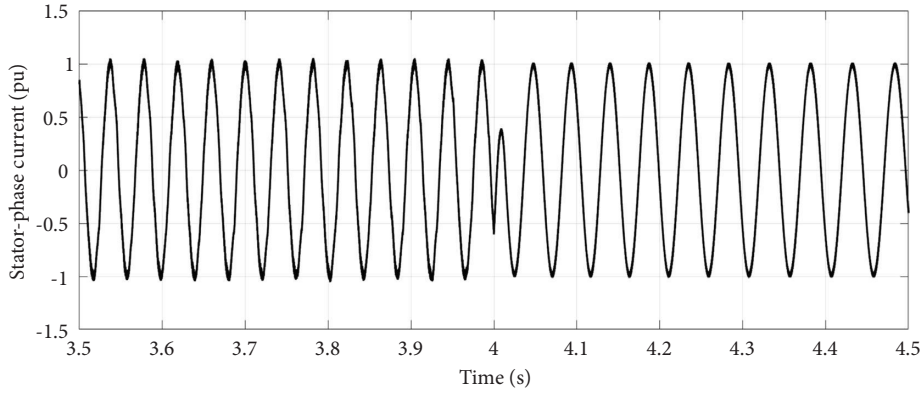

Figure 9: A small time window of motor current when $T_{ref} = -1.0$ pu.

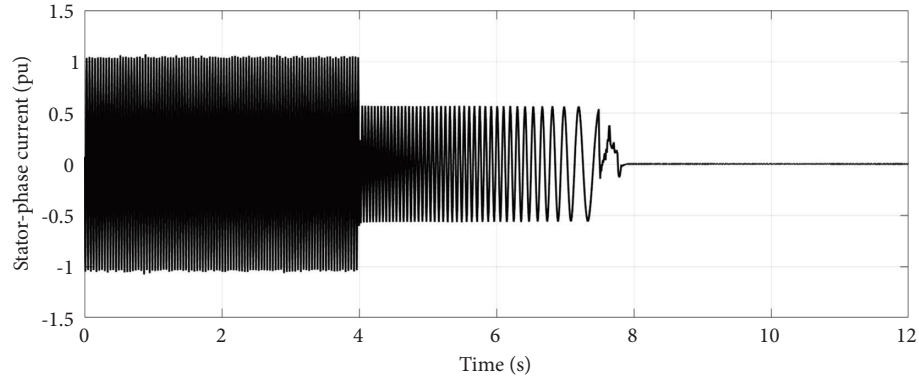

Figure 10: Motor current when $T_{ref} = -0.5$ pu.

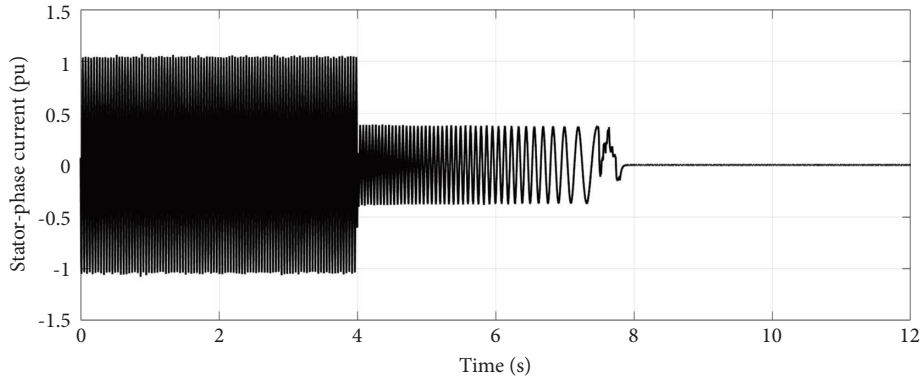

Figure 11: Motor current when $T_{ref} = -0.25$ pu.

of T_{brake}. The remaining part of T_{brake} is a friction braking torque. The values of T_{ref} are taken equal to −1.0 pu, −0.5 pu, −0.25 pu, and −0.1 pu, and the corresponding friction braking torque is equal to zero, −0.5 pu, −0.75 pu, and −0.9 pu, respectively.

Figure 4 shows the motor speed, where the braking is started at time equal to 4.0 s, and Figure 5 shows a fast and an accurate tracking of T_{ref}. This accurate tracking leads to nearly constant value of T_{brake}, equal to −1.0 pu, and therefore independent of deceleration on T_{ref}, as shown by Figure 4. Figure 6 shows the charging current of the battery, where the negative current is proportional to T_{ref}. When the LSCP is reached during deceleration of the motor, the reference values T_{ref} and $\lambda_{s,ref}$ are taken by the control and equal to zero, as shown in Figures 5 and 7. The corresponding motor currents are shown in Figures 8–12.

To show the effect of parameters uncertainty on the robustness of the control system, the results are obtained again when the stator resistance (R_s) is increased and decreased by 30%, where R_s is the only parameter which is involved in the calculations of the proposed control system. The obtained results related to T_{ref} equals to 1.0 pu are given

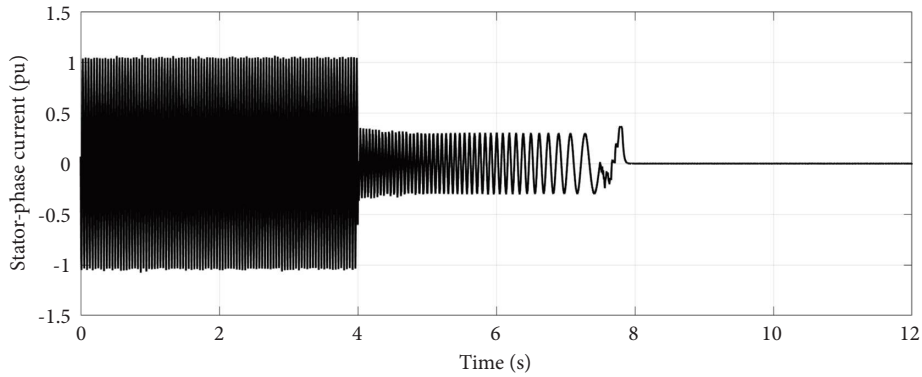

Figure 12: Motor current when $T_{ref} = -0.1$ pu.

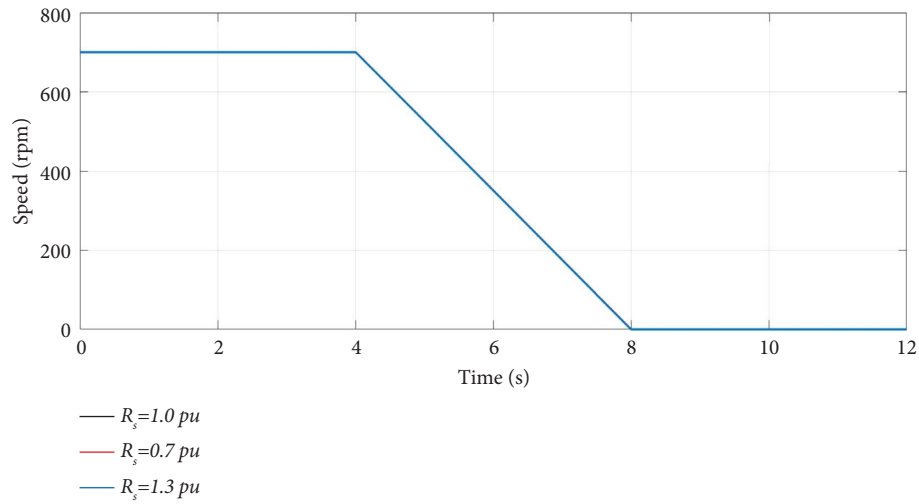

Figure 13: Motor speed when $T_{ref} = -1.0$ pu and by changing R_s.

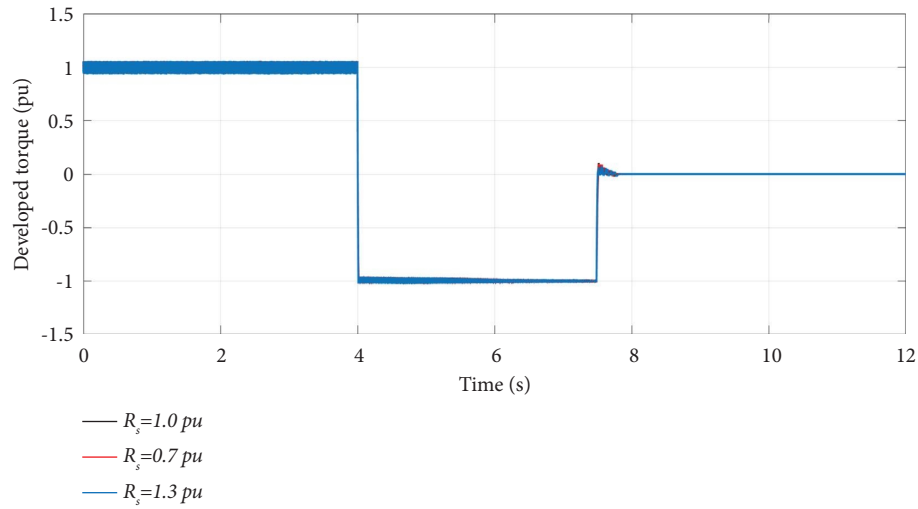

Figure 14: Developed torque when $T_{ref} = -1.0$ pu and by changing R_s.

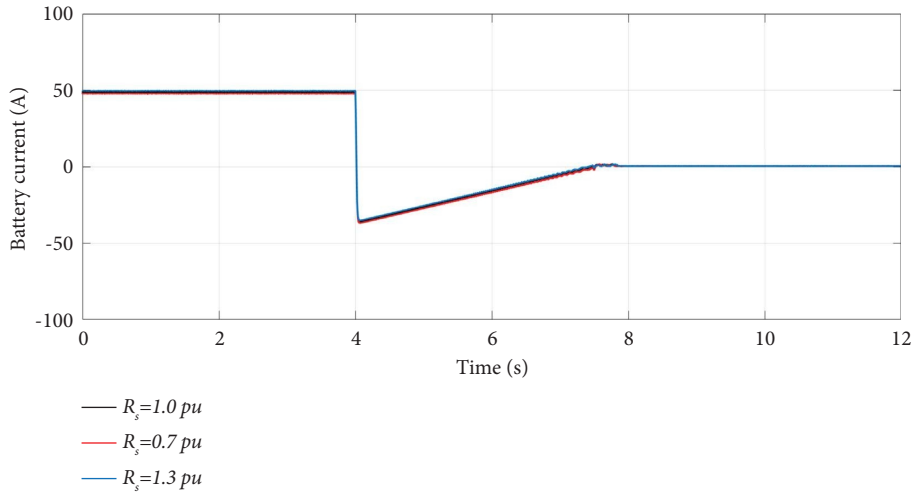

Figure 15: Battery current when $T_{ref} = -1.0$ pu and by changing R_s.

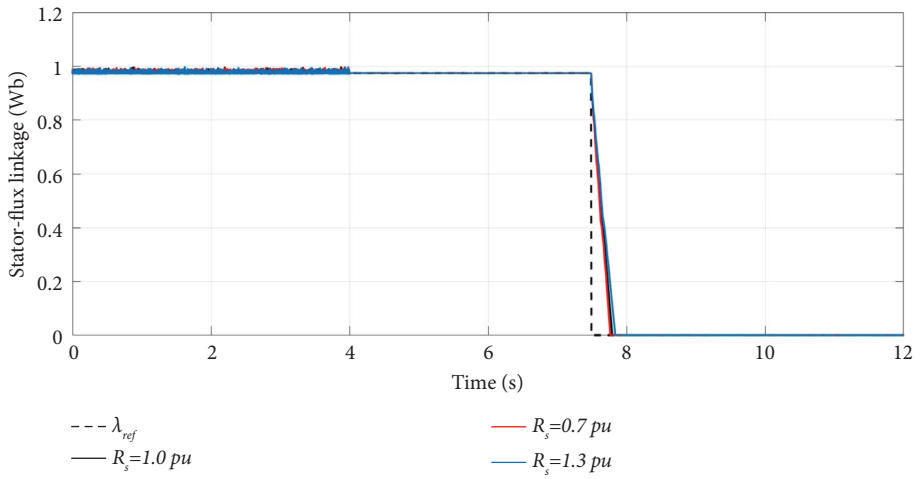

Figure 16: Stator-flux linkage when $T_{ref} = -1.0$ pu and by changing R_s.

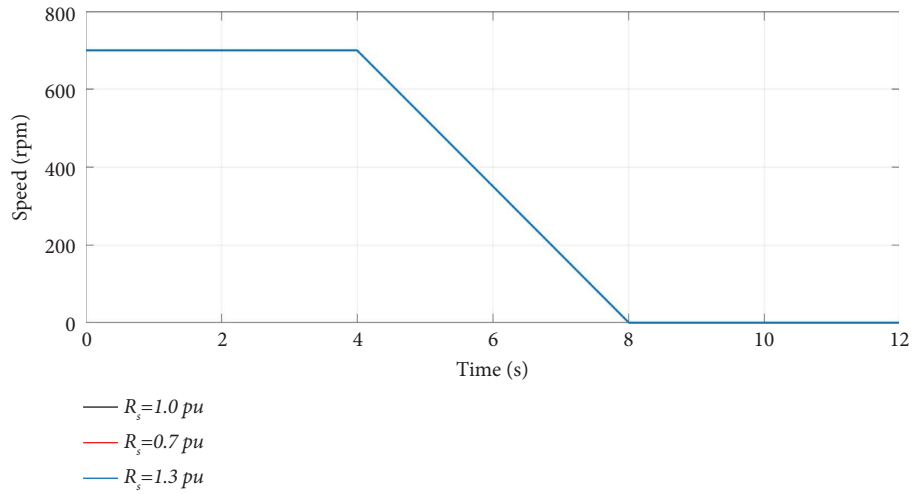

Figure 17: Motor speed when $T_{ref} = -0.1$ pu and by changing R_s.

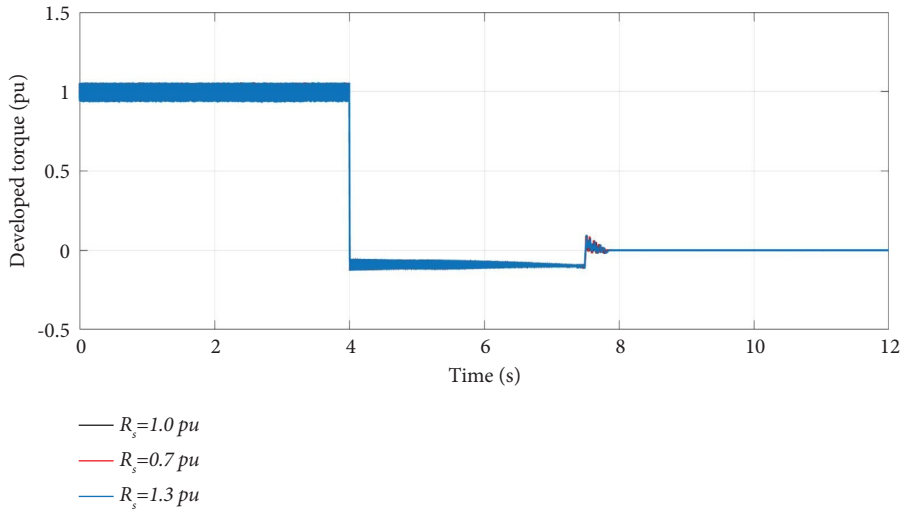

Figure 18: Developed torque when $T_{ref} = -0.1$ pu and by changing R_s.

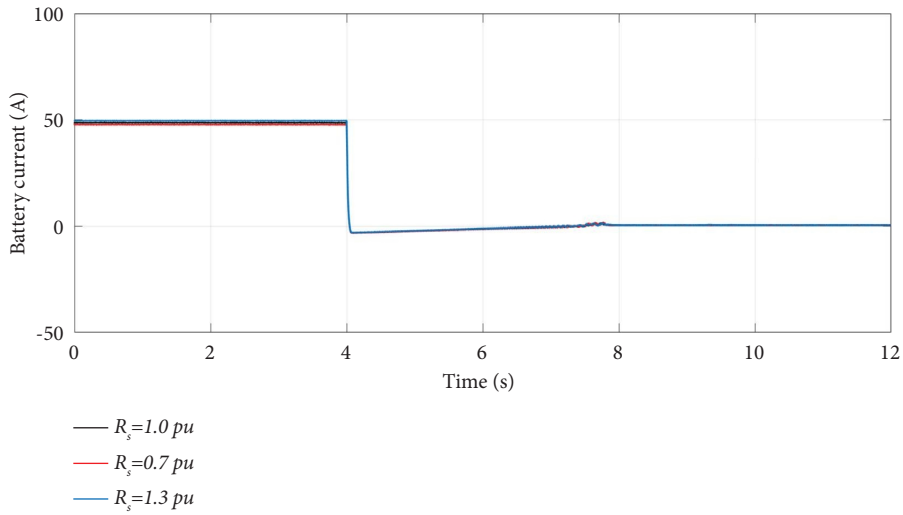

Figure 19: Battery current when $T_{ref} = -0.1$ pu and by changing R_s.

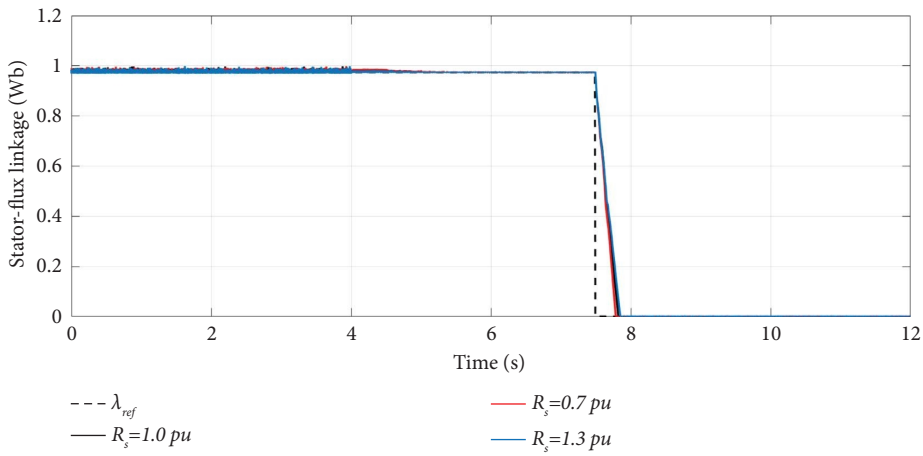

Figure 20: Stator-flux linkage when $T_{ref} = -0.1$ pu and by changing R_s.

in Figures 13–16. Furthermore, to show insignificant variation of the performance of the system, the results illustrated in Figures 17–20 are corresponding to T_{ref} equals to 0.1 pu.

5. Conclusion

Electric vehicles (EVs) need regenerative braking (RB) because it increases the efficiency of the vehicle and therefore extends the vehicle driving range. In the front-wheel drive EV, the rear braking force is only exerted by friction braking and the front-braking force is shared between the friction barking and RB, where the motor control scheme receives the appropriate reference torque (T_{ref}) signal, during RB, from a front-braking-force distribution controller. The establishing of the motor control scheme depends on the type of electrical motor used in EV. However, in EV-based IM drives, the interest was only for motor-speed control, and RB control of induction motors was absent. This paper has proposed a motor control scheme dedicated to induction motors for RB mode. The implementation of the proposed control scheme has assured a simplicity and controllability under various operating states. Moreover, the presented results have confirmed the robust behavior of the proposed control system for induction motor drives under RB mode of EVs.

6. Future Perspectives

The future of electric vehicles (EVs) holds tremendous promise, and integrating more intelligent control topology stands as a key catalyst for their advancement [33]. Intelligent control systems, encompassing sophisticated algorithms and machine learning, have the potential to optimize various aspects of EV performance. Enhanced energy management, predictive maintenance, and adaptive charging strategies are among the many benefits of intelligent control topology [34, 35]. These systems can dynamically adjust power distribution, manage battery health, and optimize charging based on real-time data and user behavior. Furthermore, intelligent control facilitates seamless communication between vehicles and infrastructure, enabling smart grid integration and grid-friendly charging. This not only enhances the overall efficiency of EVs but also contributes to grid stability and resilience. The future of electric vehicles is intricately tied to the evolution of intelligent control systems, promising a smarter, more sustainable, and user-friendly transportation landscape [36, 37].

Data Availability

The data used to support the findings of this study have not been made available.

Conflicts of Interest

The authors declare that they have no conflicts of interest.

Authors' Contributions

Omar E. M. Youssef, Mohamed G. Hussien, and Abd El-Wahab Hassan conceptualized the study, proposed the methodology, investigated the study, performed data curation, visualized the study, provided software, performed formal analysis, validated the study, wrote the original draft, and reviewed and edited the manuscript.

References

[1] S. Zhang, Z. Zhou, R. Luo, R. Zhao, Y. Xiao, and Y. Xu, "A low-carbon, fixed-tour scheduling problem with time windows in a time-dependent traffic environment," *International Journal of Production Research*, vol. 61, no. 18, pp. 6177–6196, 2023.

[2] X. Lin, Y. Wen, R. Yu, J. Yu, and H. Wen, "Improved weak grids synchronization unit for passivity enhancement of grid-connected inverter," *IEEE Journal of Emerging and Selected Topics in Power Electronics*, vol. 10, no. 6, pp. 7084–7097, 2022.

[3] X. Lin, Y. Liu, J. Yu, R. Yu, J. Zhang, and H. Wen, "Stability analysis of Three-phase Grid-Connected inverter under the weak grids with asymmetrical grid impedance by LTP theory in time domain," *International Journal of Electrical Power and Energy Systems*, vol. 142, Article ID 108244, 2022.

[4] S. Yu, C. Zhao, L. Song, Y. Li, and Y. Du, "Understanding traffic bottlenecks of long freeway tunnels based on a novel location-dependent lighting-related car-following model," *Tunnelling and Underground Space Technology*, vol. 136, Article ID 105098, 2023.

[5] J. Zhao, D. Song, B. Zhu, Z. Sun, J. Han, and Y. Sun, "A human-like trajectory planning method on a curve based on the driver preview mechanism," *IEEE Transactions on Intelligent Transportation Systems*, vol. 24, no. 11, pp. 11682–11698, 2023.

[6] W. Yue, C. Li, S. Wang, N. Xue, and J. Wu, "Cooperative incident management in mixed traffic of CAVs and human-driven vehicles," *IEEE Transactions on Intelligent Transportation Systems*, vol. 24, no. 11, pp. 12462–12476, 2023.

[7] Z. Wang, J. Li, C. Hu, X. Li, and Y. Zhu, "Hybrid energy storage system and management strategy for motor drive with high torque overload," *Journal of Energy Storage*, vol. 75, Article ID 109432, 2024.

[8] H. Chen, H. Wu, T. Kan, J. Zhang, and H. Li, "Low-carbon economic dispatch of integrated energy system containing electric hydrogen production based on VMD-GRU short-term wind power prediction," *International Journal of Electrical Power and Energy Systems*, vol. 154, Article ID 109420, 2023.

[9] X. Zhang, Y. Wang, X. Yuan, Y. Shen, Z. Lu, and Z. Wang, "Adaptive dynamic surface control with disturbance observers for battery/supercapacitor-based hybrid energy sources in electric vehicles," *IEEE Transactions on Transportation Electrification*, vol. 1, 2022.

[10] A. A. Ahmed, M. G. Hussien, and Y. M. Abo-Elyzeed, "Investigation on energy flow performance of a photovoltaic/battery-based isolated charging station for battery-powered electric vehicles," *International Transactions on Electrical Energy Systems*, vol. 2023, Article ID 4690844, 23 pages, 2023.

[11] Y. Duan, Y. Zhao, and J. Hu, "An initialization-free distributed algorithm for dynamic economic dispatch problems in microgrid: modeling, optimization and analysis," *Sustainable Energy, Grids and Networks*, vol. 34, Article ID 101004, 2023.

[12] L. Zhang, C. Sun, G. Cai, and L. H. Koh, "Charging and discharging optimization strategy for electric vehicles considering elasticity demand response," *eTransportation*, vol. 18, Article ID 100262, 2023.

[13] B. Zhu, Y. Sun, J. Zhao, J. Han, P. Zhang, and T. Fan, "A critical scenario search method for intelligent vehicle testing based on the social cognitive optimization algorithm," *IEEE Transactions on Intelligent Transportation Systems*, vol. 24, no. 8, pp. 7974–7986, 2023.

[14] L. Zhang, Q. Yin, W. Zhu et al., "Research on the orderly charging and discharging mechanism of electric vehicles considering travel characteristics and carbon quota," *IEEE Transactions on Transportation Electrification*, vol. 1, p. 1, 2023.

[15] S. Liu and C. Liu, "Virtual-Vector-based robust predictive current control for dual three-phase PMSM," *IEEE Transactions on Industrial Electronics*, vol. 68, no. 3, pp. 2048–2058, 2021.

[16] P. Wang, X. Wu, and X. He, "Vibration-theoretic approach to vulnerability analysis of nonlinear vehicle platoons," *IEEE Transactions on Intelligent Transportation Systems*, vol. 24, no. 10, pp. 11334–11344, 2023.

[17] X. Zhang, Z. Lu, X. Yuan, Y. Wang, and X. Shen, "L2-Gain adaptive robust control for hybrid energy storage system in electric vehicles," *IEEE Transactions on Power Electronics*, vol. 36, no. 6, pp. 7319–7332, 2021.

[18] M. Yang, Y. Wang, X. Xiao, and Y. Li, "A robust damping control for virtual synchronous generators based on energy reshaping," *IEEE Transactions on Energy Conversion*, vol. 38, no. 3, pp. 2146–2159, 2023.

[19] W. Hu, T. Wang, and F. Chu, "Novel ramanujan digital twin for motor periodic fault monitoring and detection," *IEEE Transactions on Industrial Informatics*, vol. 19, no. 12, pp. 11564–11572, 2023.

[20] X. Yang, X. Wang, S. Wang, K. Wang, and M. B. Sial, "Finite-time adaptive dynamic surface synchronization control for dual-motor servo systems with backlash and time-varying uncertainties," *ISA Transactions*, vol. 137, pp. 248–262, 2023.

[21] Y. Zhu, H. Wu, and J. Zhang, "Regenerative braking control strategy for electric vehicles based on optimization of switched reluctance generator drive system," *IEEE Access*, vol. 8, pp. 76671–76682, 2020.

[22] Z. Ding, X. Wu, C. Chen, and X. Yuan, "Magnetic field analysis of surface-mounted permanent magnet motors based on an improved conformal mapping method," *IEEE Transactions on Industry Applications*, vol. 59, no. 2, pp. 1689–1698, 2023.

[23] Y. Chen, "Research on collaborative innovation of key common technologies in new energy vehicle industry based on digital twin technology," *Energy Reports*, vol. 8, pp. 15399–15407, 2022.

[24] A. Flah, B. Oussama, L. Sbita, and N. S. Mohamed, "BLDC control method optimized by PSO algorithm," in *Proceedings of the 2019 International Symposium on Advanced Electrical and Communication Technologies (ISAECT)*, Rome, Italy, November 2019.

[25] A. Flah and L. Sbita, "Overview on BLAC and BLDC motors: designs and mathematical modeling," *International Journal of Powertrains*, vol. 10, no. 2, pp. 1–12, 2021.

[26] O. E. M. Youssef, M. G. Hussien, and A. E. W. Hassan, "A new simplified sensorless direct stator field-oriented control of induction motor drives," *Frontiers in Energy Research*, vol. 10, 2022.

[27] H. Wang, X. Wu, X. Zheng, and X. Yuan, "Model predictive current control of nine-phase open-end winding PMSMs with an online virtual vector synthesis strategy," *IEEE Transactions on Industrial Electronics*, vol. 70, no. 3, pp. 2199–2208, 2023.

[28] M. G. Hussien, Z. M. Salem Elbarbary, and A. E. W. Hassan, "High-performance sensorless operation of motor-generator set with an improved torque-ripple minimization strategy," *Frontiers in Energy Research*, vol. 10, 2022.

[29] O. E. M. Youssef, M. G. Hussien, and A. E. W. Hassan, "An advanced control performance of a sophisticated stand-alone wind-driven DFIG system," *International Transactions on Electrical Energy Systems*, vol. 2023, Article ID 5541932, 11 pages, 2023.

[30] Y. Lu, C. Tan, W. Ge, Y. Zhao, and G. Wang, "Adaptive disturbance observer-based improved super-twisting sliding mode control for electromagnetic direct-drive pump," *Smart Materials and Structures*, vol. 32, no. 1, Article ID 017001, 2023.

[31] X. Zhang, W. Pan, R. Scattolini, S. Yu, and X. Xu, "Robust tube-based model predictive control with Koopman operators," *Automatica*, vol. 137, Article ID 110114, 2022.

[32] B. Xu and Y. Guo, "A novel DVL calibration method based on robust invariant extended kalman filter," *IEEE Transactions on Vehicular Technology*, vol. 71, no. 9, pp. 9422–9434, 2022.

[33] M. G. Hussien, "A new robust sensorless vector-control strategy for wound-rotor induction motors," *Australian Journal of Electrical and Electronics Engineering*, vol. 17, no. 2, pp. 132–137, 2020.

[34] N. Mohamed, F. Aymen, B. H. Mouna, and S. Lassaad, "Modeling and simulation of vector control for a Permanent Magnet Synchronous Motor in electric vehicle," in *Proceedings of the 2021 4th International Symposium on Advanced Electrical and Communication Technologies, ISAECT 2021*, no. 1, pp. 1–5, Alkhobar, Saudi Arabia, December 2021.

[35] H. Kraiem, A. Flah, N. Mohamed et al., "Increasing electric vehicle autonomy using a photovoltaic system controlled by particle swarm optimization," *IEEE Access*, vol. 9, pp. 72040–72054, 2021.

[36] U. Salahuddin, H. Ejaz, and N. Iqbal, "Grid to wheel energy efficiency analysis of battery- and fuel cell–powered vehicles," *International Journal of Energy Research*, vol. 42, no. 5, pp. 2021–2028, 2018.

[37] C. S. Ernst, A. Hackbarth, R. Madlener, B. Lunz, D. Uwe Sauer, and L. Eckstein, "Battery sizing for serial plug-in hybrid electric vehicles: a model-based economic analysis for Germany," *Energy Policy*, vol. 39, no. 10, pp. 5871–5882, 2011.